A Comparative Study of Distinct Advanced MPPT Algorithms for a PV Boost Converter

Mohamed Ali Zdiri*‡, Badreddine Khelifi*,**, Fatma Ben Salem*, and Hsan Hadj Abdallah*

* Control & Energy Management Laboratory (CEMLab)

University of Sfax, Sfax Engineering School, BP 1173, 3038 Sfax, Tunisia

** IEEE senior member

(mohamed-ali.zdiri@enis.tn, badr.khelifi@ieee.org, fatma.bensalem@enis.rnu.tn, hajabdallahhsan@gmail.com)

‡ Corresponding Author; Mohamed Ali Zdiri, Control & Energy Management Laboratory, ENIS, University of Sfax

Received: 24.05.2021 Accepted:19.06.2021

Abstract- PV energy are enticing an enormous focus in the actual energy scenario. In order to assure the transfer of the maximum power to the load, a boost converter is used containing several MPPT techniques. In this paper, the comparative analysis of the system dynamic behavior has been perform based in distinct MPPT techniques, which are P&O, FLC, ANN-PI and ANN-SM. Taking into account the results of these techniques, the ANN-SM based MPPT controller can attain the MPP rapid than the other MPPT techniques under various climatic condition and load. It is also confirmed that the ANN-SM algorithm has a low ripple rate in power compared with the P&O MPPT controller. Furthermore, the ANN-SM MPPT approach requires fewer dissipated energies than the other techniques. In conclusion, the ANN-SM dynamic behavior illustrates that the PV system stay attain the MPP during load and climatic condition variations with high performances and efficiency.

Keywords PV energy, MPPT techniques, P&O, FLC, ANN-PI, ANN-SM, Dynamic behavior.

1. Introduction

Renewable energy sources, such as photovoltaic and wind energy, have recently been used in a variety of industrial applications due to their accessibility and environmental friendliness. In Tunisia, the photovoltaic energy exploitation is estimated to a few hundred gig-watt (GW) according to NAEM (National Agency for Energy Management). In the same context, the average global horizontal radiation in Tunisia is equal to 1850 kWh/m², which explains an average annual photovoltaic production in the order of the value of 1650 kWh/kWp. Accordingly, the PV energy is well regarded as a hopeful green energy source. Indeed, the PV systems have distinct drawbacks such as the low efficiency of the energy conversion and the high price of the fabrication [1]. In order to avoid these drawbacks and to increase the PV systems efficiency, a MPPT controller must be used by extracting the maximum power towards the load [2-3]. A DC/DC converter is required to use these MPPT methods. This converter type is susceptible to a variety of problems, including open-circuit and short-circuit failures [4]. The MPPT approaches deliver the greatest power to the load while taking into account the PV system's metrological fluctuation [5-11]. Furthermore, in PV systems, the solar panel is a critical component for generating power [12]. In general, the role of the MPPT techniques is the extraction of the MPP even with the climatic condition variations in order to supply the load by the maximum power [13-15].

During the climatic condition and load variations, the MPPT techniques try to modify the duty cycle in accordance with these variations [16]. During these last years, considering the technological development, several researchers have created several MPPT techniques. Moreover, these MPPT techniques are classified into distinct categories, which are: voltage feedback, hill climbing, current feedback, P&O, IC, neural network and fuzzy logic [17-18]. In this context, an inexpensive current based MPPT technique has been presented in [19]. Taking into account the presented methods, the voltage feedback and hill climbing have advantage such as the ease of satisfaction, however, it have disadvantages the example of the inefficient of tracking the MPP under climatic condition variations. The other hand, the P&O MPPT technique has attached by a PI control loops, which product a sluggish MPP tracking procedure [20-21]. The ANFIS algorithm is the most effective MPPT method in terms of tracking the MPP even under the variations of the climatic condition and load. In more detail, the ANFIS algorithm combine the performance of the fuzzy logic and neural network as addressed in [22-25]. Moreover, the ANN-SM MPPT technique is presented in order to decrease the

MPP tracking time. This is achieved by combining the SM and the neural network which show the high performance and efficient in terms of the MPP tracking speed [26].

In this paper, a MPPT techniques behavior comparison of the P&O, FLC, ANN-PI and ANN-SM has been presented. The outcomes of simulation prove to confirm the performance and efficient of the ANN-SM comparing to the other existing MPPT techniques in terms of MPP tracking speed, fewer dissipated energies and low ripple rate even under the variations of the climatic condition and load.

2. Description and modelling of the photovoltaic system including MPPT algorithms

The studied PV system is composed by a PV generator, DC/DC boost converter controlled by a MPPT technique and a DC load as presented in Fig. 1.

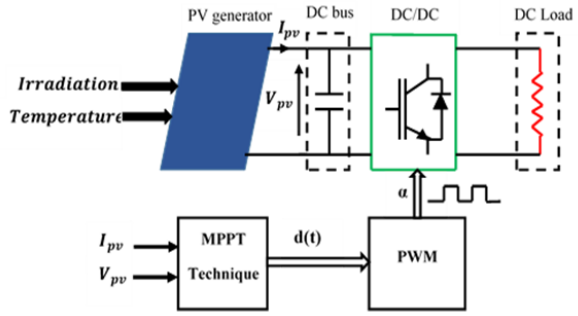

Fig. 1. Block diagram of the PV system.

The following section is focused on the modelling of all PV system elements in more detail.

2.1. Photovoltaic generator modelling

A photovoltaic generator is composed by several photovoltaic module in order to meet the energy requirements of the loads. In the same context, a PV module is a set of the association of several solar cells. In this paper, an equivalent circuit consists of a single diode is used as presented in Fig. 2. The determination of their internal parameters is presented in [27]. A photovoltaic generator (PV generator) is a piece of equipment that uses photovoltaic energy to satisfy load demands. A photovoltaic module is made up of a group of solar cells that are connected in parallel and/or series.

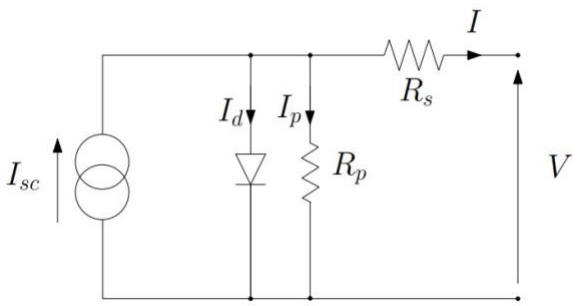

Fig. 2. PV solar cell circuit with a single diode.

The I current expression is presented by the following expression:

$$I = I_{sc} - I_d - I_p \tag{1}$$

Where:

$$I_{pv} = \frac{V + R_s I}{R_p} \tag{2}$$

And

$$I_d = I_0[\exp(\frac{qV_d}{KT}) - 1] \tag{3}$$

Where:

$$V_d = \frac{V + R_s I}{a} \tag{4}$$

Where: I denotes the PV solar cell current, V: the PV cell voltage, I_{sc}: the short circuit current of the photovoltaic cell, R_p and R_s: the shunt and serie resistances, I_0: the PV cell saturation current, K: the constant of Boltzmann = 1.381x 10^{-23} (J/K), T: the PV cell temperature, a: the ideality factor and q: the electron charge equal to 1.6 10^{-19} C.

The PV cell characteristic (current-voltage) is given by:

$$I = I_{sc} - I_0[\exp[\frac{q(V + R_s I)}{aKT}] - 1] - \frac{V + R_s I}{R_p} \tag{5}$$

Where the I_{sc} current is expressed by:

$$I_{sc} = \frac{R_p + R_s}{R_p} I_{pv} \tag{6}$$

Considering this condition $I_{sc} = I_{pv}$, which is utilized in order of optimization, the I current can be defined as follows:

$$I = I_{pv} - I_0[\exp(\frac{q(V + R_s I)}{aV_t}) - 1] - \frac{V + R_s I}{R_p} \tag{7}$$

Where the V_t voltage is given by:

$$V_t = \frac{N_s KT}{q} \tag{8}$$

With N_s represents the series cells number.

The PV generator current I_{pv} depends essentially on the climatic conditions variations as given by [27]:

$$I_{pv} = (I_{pv,n} + K_i \Delta T)\frac{G}{G_n} \tag{9}$$

Where $\Delta T = T\text{-}T_n$, $I_{pv,n}$: the light induced current, G_n represents the G irradiation at the nominal condition and K_i denotes the coefficient of the current/temperature. Based on the equation (3) and (4), the I_d current is given by:

$$I_d = I_0[\exp(\frac{q(V + R_s I)}{aV_t}) - 1] \tag{10}$$

Where:

$$I_0 = \frac{I_{sc,n} + K_i \Delta T}{\exp(\frac{q(V_{oc,n} + K_i \Delta T)}{aV_t}) - 1} \tag{11}$$

With the $I_{sc,n}$ current and the $V_{oc,n}$ voltage denote the short circuit current and the open circuit voltage at the nominal condition, respectively.

Taking into account the $I_{pv,m}$ current as:

$$I_{pv,m} = I_{pv} - I_d \tag{12}$$

Accordingly, we obtain:

$$I_{pv,m} = I_{pv}N_{pp} - I_0 N_{pp} \exp[\frac{qTN_{ss}}{aKN_s}(V + \frac{IR_s}{N_{pp}}N_{ss}) - 1] \quad (13)$$

Where N_{ss} and N_{pp} denote the series and parallel PV modules numbers, respectively.

In order to provide the maximum amount of power to the load, a DC/DC power converter must be used. Accordingly, the following sections detailed more the used converter with their MPPT techniques.

2.2. Boost converter modelling

The used DC/DC power converter is a boost converter, which means that the output voltage is always greater than the input voltage. The electrical circuit of the boost converter is presented in Fig. 3. Indeed, this converter is composed by an input voltage source V_{pv}, an inductor L, an IGBT *d*, a diode D, an input capacitor C_1 and output capacitor C_2.

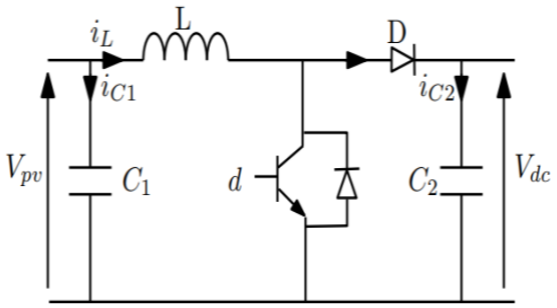

Fig. 3. Boost converter circuit.

At the steady state, the transfer function of the used converter is given by equation (14):

$$V_{dc} = \frac{V_{pv}}{1 - d(t)} \quad (14)$$

Where: d(t) denotes the duty cycle.
Furthermore, the inductance L is obtained basing on the desired of the ripple amplitude Δi_L, which is expressed by:

$$L = \frac{dV_{pv}}{f\Delta i_L} \quad (15)$$

Where f represents the switching frequency. Moreover, C_1 and C_2 (the input and output capacitors) are expressed in function of the desired of the ripples amplitudes ΔV_{pv} and ΔV_{dc}, respectively, as follows:

$$\begin{cases} C_1 = \dfrac{dV_{pv}}{8L\Delta V_{pv} f^2} \\ C_2 = \dfrac{di_{dc}}{f\Delta V_{dc}} \end{cases} \quad (16)$$

2.3. MPPT techniques

Under the irradiation and temperature variations, the MPP varies according to these variations. Therefore, it must be applied these MPPT techniques in order to transfer the maximum amount of electric power to the load while taking into consideration the climatic condition and load variations.

In this paper, we focus only on four MPPT methods, which are:

- P&O,
- FLC,
- ANN-PI, and
- ANN-SM.

2.3.1. P&O technique

The P&O technique is extensively used in practical implementation due to their simplicity and efficacy. This technique is founded on the disturbance of the PV voltage and compare this latter with the new voltage after disturbance. Indeed, the P&O finds the MPP even with the climatic condition and load variations. The P&O technique flowchart is presented in Fig. 4 [28].

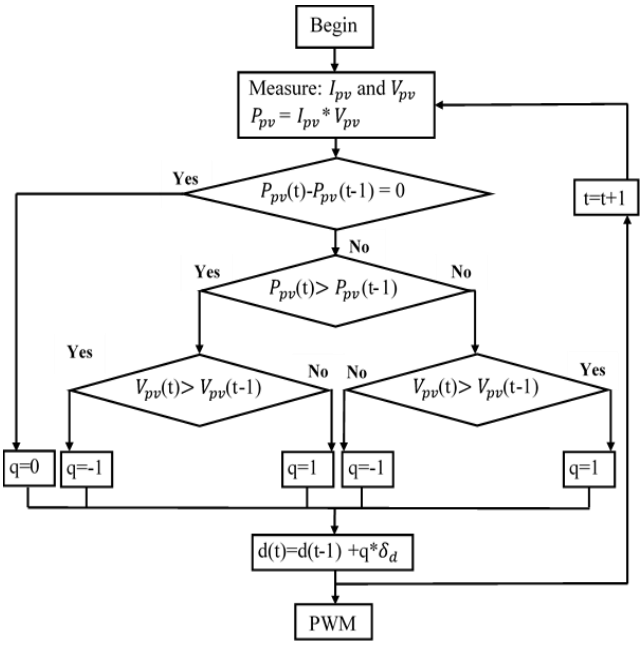

Fig. 4. P&O technique flowchart.

2.3.2. FLC

The FLC control the PV system basing on the data knowledge. Indeed, the FLC modules are classified into:

- Fuzzification,
- Decision making, and
- Defuzzification.

The structure of the FLC block is presented in Fig. 5.

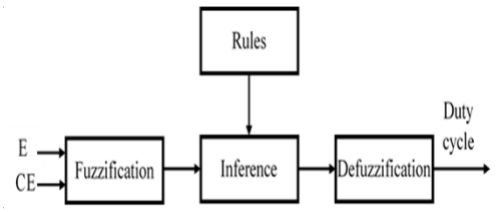

Fig. 5. FLC block diagram.

The FLC bloc inputs are E and CE, which are presented by equation (17). Indeed, the FLC bloc output is the duty cycle.

$$\begin{cases} E = \dfrac{P_{pv}(k) - P_{pv}(k-1)}{V_{pv}(k) - V_{pv}(k-1)} \\ CE = E(k) - E(k-1) \end{cases} \quad (17)$$

Where k denotes the sample time.

For more explaining, the fuzzification process, fuzzy inference process and defuzzification process are presented as follows:

- **Fuzzification:** the process of fuzzification needs that each used variable to describe the control rules must be written in terms notations of fuzzy set along with linguistic labels. The MF's of the inputs and output variables (E(k), CE(k) and duty cycle) are illustrated in Fig. 6. Indeed, the PWM bloc uses the duty cycle in order to control the boost converter switch. Each FLC inputs and output are composed by a five fuzzy sets, which are: LL, HL, ZE, LH and HH (where: L and H represent low and high, respectively) as presented in Fig. 6.
- **Inference:** the inference method is the step of formulating the cartography using FLC of a given input to an output. In this paper, we used a fuzzy inference of type Mamdani. Furthermore, Table 1 illustrates the table of rules.
- **Defuzzification:** the defuzzification process computes the FLC crisp output. In this work, the defuzzifier of type center of gravity is adopted.

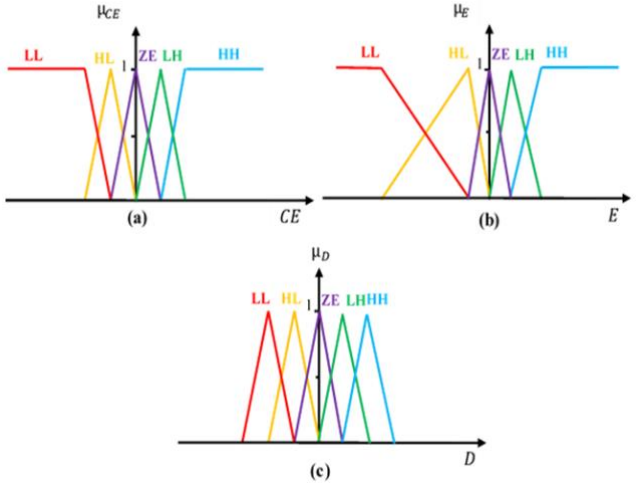

Fig. 6. Inputs and output MF's. **Legend:** (a): μ_{CE}, (b): μ_E and (c): μ_D.

Table 1. Rules table.

CE	E				
	LL	HL	ZE	LH	HH
LL	HH	HH	LH	HH	HH
HL	HH	LH	LH	LH	HH
ZE	HL	HL	ZE	LH	LH
LH	LL	HL	HL	HL	LL
HH	LL	LL	HL	LL	LL

2.3.3. ANN-PI

Recently, ANN-PI technique has attracted many interests in the tracking of the PV systems MPP. It is underlined that this technique is based on the ANN in order to resolving complex problems. The ANN technique is composed by two important stages, which are the training stage and the operational stage. The ANN model is shown in Fig. 7. Referring to this figure, the ANN model's inputs and output are the temperature, irradiance and the reference maximum power $P_{gp\max}$, respectively.

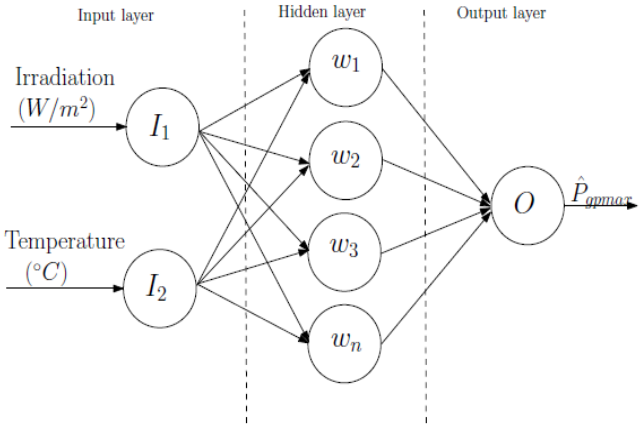

Fig. 7. ANN block diagram.

The ANN model determines the reference power considering the climatic condition variations. The used ANN model is developed using MATLAB/Simulink environment. A feedforward NN composed by two neurons, five neurons and one neuron in the input layer, hidden layer and output layer, respectively, is used as presented in Fig. 8.

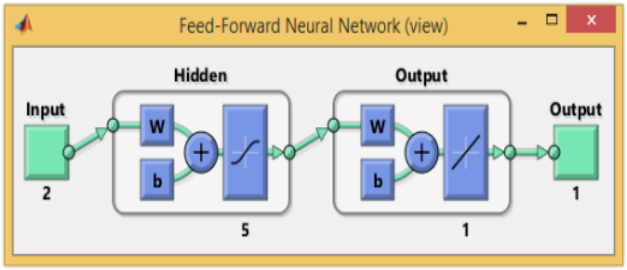

Fig. 8. MATLAB feedforward NN model.

After this step, the PI controller is utilized in order to determine the difference in maximum power between the reference and measured values. The PI controller is illustrated in Fig. 9. The PI controller purpose is utilized to reduce the error value, which can be expressed by the following equation:

$$u(t) = K_p e(t) + K_i \int_0^t e(t')dt' \quad (18)$$

Where K_p and K_i denote the coefficients of the PI controller [29].

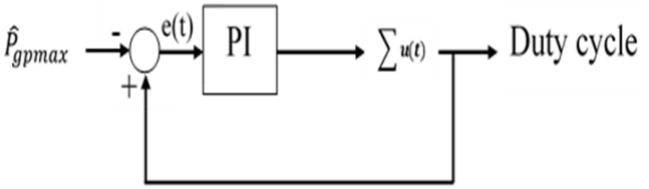

Fig. 9. PI controller block diagram.

Indeed, a PWM bloc uses the duty cycle (the output of the PI controller) to control the boost converter switch (ON state or OFF state).

2.3.4. ANN-SM

The control discontinuous aspect specifying a desirable dynamic of the system characterizes VSC and their sliding regimes (dubbed Sliding Modes SM). Such dynamics are achieved by selecting suitable variety spaces, also known as sliding surfaces controllers provide sufficient switching, and resulting in the closed loop systems desired behavior.

Consider the structure defined by the state equation below [30]:

$$\dot{Y}(t) = FY + BU \tag{19}$$

Where: $Y \in R^n$ denotes the state vector and $U \in R^m$ is the vector of control. The SM control action is expressed as:

$$U = U_{eq} + \Delta U \tag{20}$$

Where: U_{eq} represents the so-called equivalent control to get to and stay on the sliding surface S(Y) = 0. The ΔU term corresponds to the required term to have a steady PV system external the sliding surface, even in the case of bad-modeled systems and external disturbances.

- Design of the sliding surface:

The sliding function S(Y) should be chosen in such away: when S(Y) = 0, Y goes to the desired state Y. The basic principle of the SM controllers consists to oblige the system to reach the sliding surface and to remain on it. That is: S(Y) = 0, and then: $\dot{S}(Y) = 0$.

$$S(Y) = (\frac{\partial}{\partial Y} + \lambda)^{j-1}(\hat{Y} - Y) \tag{21}$$

With: j represents the time number to derive the surface in order to obtain the control and λ is a positive constant.

- Equivalent control writing:

$$\dot{S}(Y) = \frac{\partial S}{\partial Y}[F(Y) + B(Y)U(t)] = 0 \tag{22}$$

And under the regularity of matrix $\frac{\partial S}{\partial Y}B(Y)$, yields:

$$U_{eq} = -\left(\frac{\partial S}{\partial Y}B(Y)\right)^{-1}\frac{\partial S}{\partial Y}F(Y) \tag{23}$$

- The discontinuous term of the control is chosen as:

$$\Delta U = -\left(\frac{\partial S}{\partial Y}B(Y)\right)^{-1}U_0 sign(S) \tag{24}$$

Where: U_0 is a definite diagonal matrix of positive value.

Considering the following Lyapunov function:

$$V_l(x) = \frac{1}{2}S^T S > 0 \tag{25}$$

Its derivative in function of time results in:

$$\dot{V}_l(x) = S^T \dot{S} = S^T \frac{\partial S}{\partial X}[F(X) + B(X)U(t)]$$

$$= S^T \frac{\partial S}{\partial X}[F(X) + B(X)(U_{eq} + \Delta U)]$$

$$= S^T \frac{\partial S}{\partial X}B(X)\Delta U$$

$$= -S^T U_0 signS$$

$$= U_0|S| < 0 \tag{26}$$

Then, the control laws (20, 23 and 24) stabilize system (19) [31-32].

The PI controller used in the previous work is substituted by SM controller. In fact, the sliding function S (X) is considered as follows:

$$S(X) = (\hat{P}_{gp\max} - P_{gp}) + \lambda\int(\hat{P}_{gp\max} - P_{gp})dt \tag{27}$$

With P_{gp} is the power delivered by the controlled generator power.

The equation of the switching state or the switching duty cycle U (U=d) is:

$$U = U_{eq} - U_0 sign(S) = 1 - U_0 sign(S) \tag{28}$$

With U_0 illustrates a positive gain. Then the equation of switching state is in the following equations system:

$$\begin{cases} U = 0 & if \quad S > 0 \\ U = 1 & if \quad S < 0 \end{cases} \tag{29}$$

3. Simulation results

For an effective comparative study of the various MPPT techniques, the system dimension is founded on the security norms needs. Furthermore, Fig. 10 depicts the suggested Simulink model of the PV system, which includes the MPPT techniques employed. The electrical parameters of the photovoltaic generator and the boost converter are presented in Tables 2 and 3.

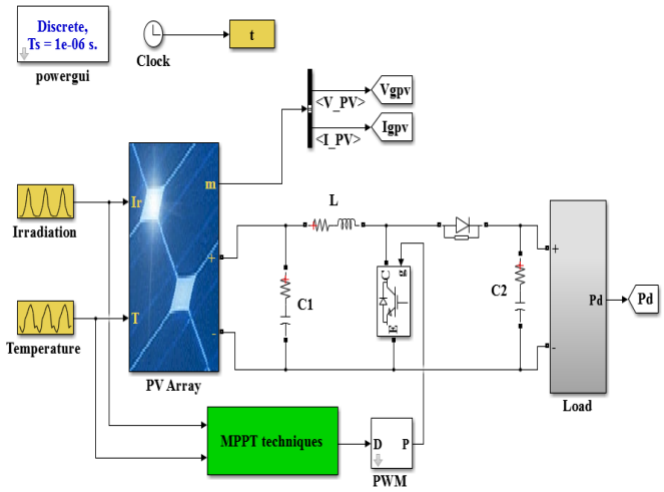

Fig. 10. MATLAB Simulink model diagram.

The PV generator is composed by 4 modules connected in series with 5 parallel strings. This PV generator produces a 1 kW energy. Kyocera LA361651 is the used PV panel

model as illustrated in Table 2. Furthermore, the boost converter parameters is illustrated in Table 3.

Table 2. The Kyocera LA361651 PV panel's settings.

Description	Value
Solar irradiation (G_n)	1000 W/m^2
Temperature norms (T_n)	25 °C
Maximum power (P_{max})	51 W
Max power voltage (V_{pmax})	16.9 V
Peak current (I_{pmax})	3.02 A
Current of short-circuit (I_{sc})	3.25 A
Voltage of open-circuit (V_{oc})	21.2 V

Table 3. Boost converter parameters.

Description	Value
Input capacitor C_1	440 µF
Inductance L	47 µH
Switching frequency f	20 kHz
Output capacitor C_2	1100 µF

In the healthy operating conditions, the maximum power point (MPP) of the PV generator current, voltage and power change according to the climatic condition variations as presented in Fig. 11.

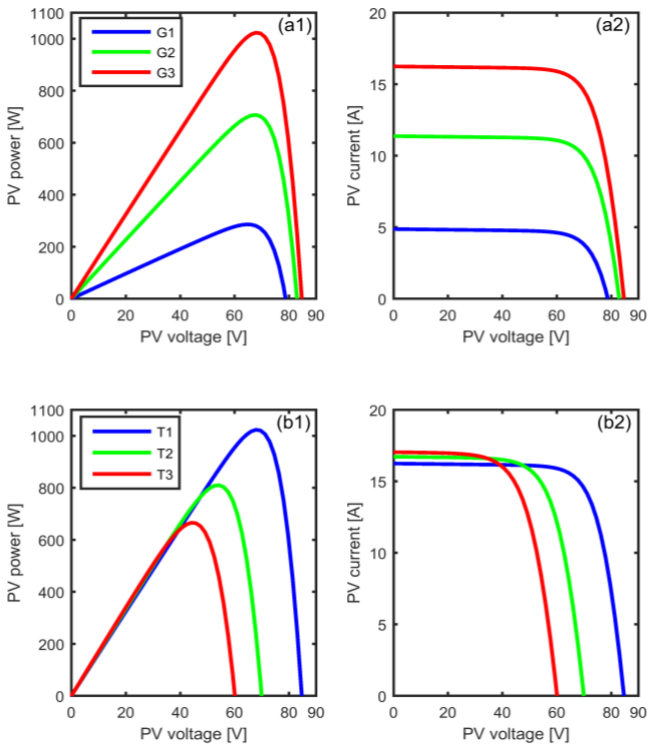

Fig. 11. Simulation results of the PV generator characteristics effects under climatic conditions variations. **Legend:** (a1) and (a2): power-voltage and current-voltage during irradiation variations (G_1, G_2 and G_3), (b1) and (b2): power-voltage and current-voltage during temperature variations (T_1, T_2 and T_3).

Referring to Fig. 11-(a1) and 11-(a2), the MPP PV generator current, voltage and power increase (decrease) with the increase (the decrease) of the irradiation. It is to be underlined that G_1, G_2 and G_3 are equal to 300 W/m^2, 600 W/m^2 and 1000 W/m^2, respectively. In the case of the temperature increase (decrease) as presented in Fig. 11-(b1) and 11-(b2), the MPP of the PV generator voltage and power decrease (increase), however, the current register a slightly increase (decrease). The values of T_1, T_2 and T_3 are equal to 25 °C, 55 °C and 75° C, respectively. In order to extract the maximum power to the resistive load, we use a boost converter to apply these distinct MPPT techniques. The used DC/DC power converter in this work is of type boost, which the output voltage always superior to the PV generator voltage.

In this simulation section, we are focused on the MPPT techniques, which are P&O, FLC, ANN-PI and ANN-SM. Moreover, Fig. 12 presents the PV generator outputs (V_{gpv}, I_{gpv} and P_{gpv}) under standard climatic condition (T=25 °C and G= 1000 W/m^2).

To study and analyze the dynamic behavior of the studied MPPT techniques, the resistor load is equal to 30 Ω keeping the irradiance and temperature in the standard state. Referring to Fig. 12, the MPP of all MPPT techniques try the same trajectory just the difference at the level of the ripple rate and rapidity. Furthermore, one can underline that the P&O command has a large ripple of the PV generator voltage (zoomed area) in comparison to the others that are currently available (FLC, ANN-PI and ANN-SM). The ANN-SM has a low ripple compared with the others studied MPPT techniques. Indeed, the ANN-SM and ANN-PI have fastest on the time response (zoomed area).

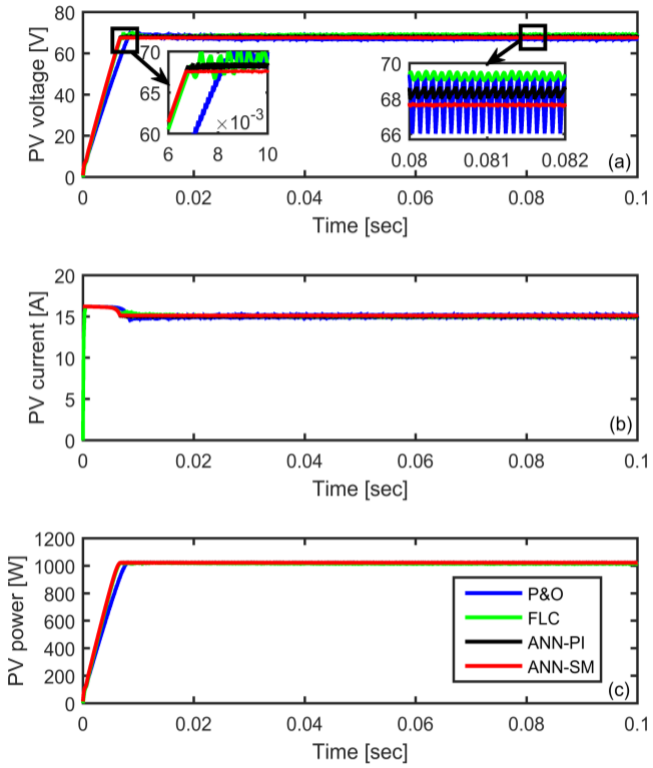

Fig. 12. PV generator outputs under standard climatic conditions with a resistive load equal to 30 Ω.

In order to study the photovoltaic system dynamic behavior, we have tested the PV system during a day with the following climatic condition and load variations as addressed in Fig. 13. Indeed, the PV generator power and current and the load power under these variations of the climatic condition and load are presented in Fig. 14.

Considering these variations, the MPP of all MPPT techniques try the same trajectory. For example, at the instant t = 13^h.01 (G = 978.6 W/m^2 and T = 23.01 °C), the PV generator power and current, as well as the load power are equal to 1014 W, 14.40 A and 700 W, respectively. Referring to Fig. 14, the ripple rate of the P&O command has a large ripple comparing to the others techniques. It is to be noted that the ANN-SM has a low ripple (zoomed area) comparing to the others MPPT techniques. Moreover, as compared to other MPPT methods, the ANN-PI and ANN-SM provide quicker response times. As conclusion, the ANN-SM has a low ripple rate and faster time on the response, which prove their high dynamic performance comparing to the others existing MPPT techniques.

In order to study the power losses of these MPPT techniques a results of simulation were performed. The oscillations minimization reflects a minimization of the energy loss. Indeed, considering the energy of the PV power error ($\varepsilon_{P_{gp}} = \hat{P}_{gp} - P_{gp}$, $P_{gp} \in \Re$) , as expressed by:

$$E_P = E_0 \int_{t_0}^{t_0+T} \varepsilon_{P_{gp}}^2 \, dt \tag{30}$$

Where E_0 is a constant value.

Since the P&O controller gives the worst case of oscillations, the comparison would be between the other three intelligent MPPT techniques namely: FL-MPPT, PI-ANN-MPPT and SM-ANN-MPPT.

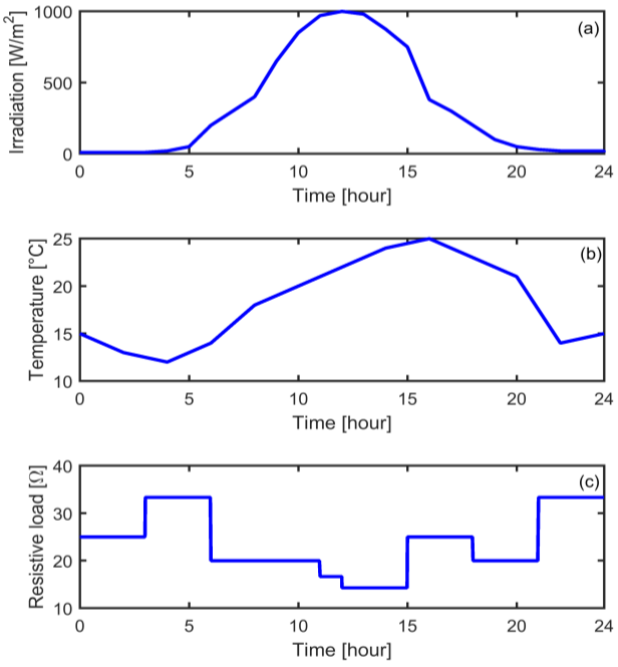

Fig. 13. Climatic condition and resistive load variations during a day.

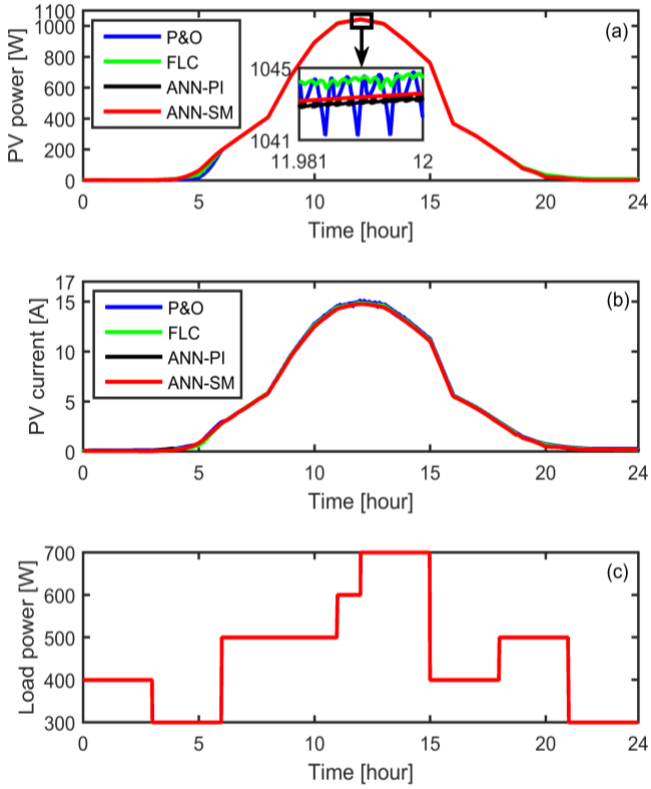

Fig. 14. Simulation results of the PV generator power, PV generator current and the load power under climatic condition and resistive load variations during a day.

The ratio $R1_{Ep}$ of the energy of the PV power error given by the FL-MPPT controller by the one given by the PI-ANN-MPPT controller is expressed by the following equation:

$$R1_G = \frac{E_P(FL-MPPT)}{E_P(PI-ANN-MPPT)} \tag{31}$$

The ratio $R2_{Ep}$ of the energy of the PV power error given by the FL-MPPT controller by the one given by the SM-ANN-MPPT controller:

$$R2_G = \frac{E_P(FL-MPPT)}{E_P(SM-ANN-MPPT)} \tag{32}$$

In Table 4 the energy ratios, between FL-MPPT, PI-ANN-MPPT, SM-ANN-MPPT techniques, is given for different irradiation levels (the temperature is fixed at 25 °C). One can notice that the SM-ANN-MPPT approach requires less dissipated energies compared to the others one. For example, the energy is almost 35 times smaller using the SM-ANN-MPPT controller for the case of G = 1000 W/m^2 comparing to the FL-MPPT.

Table 4. Energy ratio for different irradiation levels.

G (W/m²)	**100**	**500**	**1000**
Ep(FL-MPPT)	0.0051	0.0664	0.2369
Ep(PI-ANN-MPPT)	0.0876	0.0445	0.1955
Ep(SM-ANN-MPPT)	0.0001	0.0019	0.0068
$R1_G$	0.0580	1.4932	1.2122
$R2_G$	93.5283	34.7765	35.0012

4. Conclusion

In this paper, four MPPT techniques for PV generator system are successfully compared and presented. The first MPPT technique is a conventional algorithm, which is P&O, while the others MPPT techniques are intelligent algorithms, which are FLC, ANN-PI and ANN-SM.

The performance evaluation of these MPPT techniques are validated using a boost converter in order to provide the most power to the resistive load. Based on the simulation results and taking into account the variations in climatic condition and load power, the ANN-SM can produce more energy power with a low ripple rate and rapidity on the time response comparing to others existing MPPT techniques. Furthermore, the ANN-SM approach requires fewer dissipated energies than the other techniques. For example, the energy is almost 35 times smaller using the ANN-SM controller for the case of G = 1000 W/m^2 comparing to the FLC technique.

It is concluded that the ANN-SM has a better dynamic performance comparing to the others MPPT techniques in terms of MPP tracking speed, fewer dissipated energies and low ripple rate even under the climatic condition and load variations.

Appendix

PV: Photovoltaic;
P&O: Perturb and observation;
IC: Incremental conductance;
FLC: Fuzzy logic controller;
ANN: Artificial neural network;
PI: Proportional integral;
SM: Sliding mode;
MPPT: Maximum power point tracking;
MPP: Maximum power point;
IGBT: Insulated gate bipolar transistor;
E: Error;
CE: Change in error;
MF's: Membership functions;
ZE: Zero Equivalent;
VSC: Variable structure Control; and
PWM: Pulse with modulation.

References

[1] V. M. Kumaresh, R. N. Malhotra, and P. R. Saravana, "Literature Review on Solar MPPT Systems," Advance in Electronic and Electric Engineering, Vol. 4, No. 3, pp. 285-296, 2014.

[2] A.Belkaid, I.Colak, and K. Kayisli, "A comprehensive study of different photovoltaic peak power tracking methods," 6th International Conference on Renewable Energy Research and Applications (ICRERA), San Diego, CA, 5-8 Nov, pp. 1073-1079, 2017.

[3] H. Dilovan, and N. Genc, "Fuzzy and P&O Based MPPT Controllers under Different Conditions," 7th International Conference on Renewable Energy Research and Applications (ICRERA), IEEE, 2018.

[4] M.A. Zdiri, M. Ben Ammar, B. Bouzidi, A. Rabhi, and H.H. Abdallah, "An Advanced Switch Failure Diagnosis Method and Fault Tolerant Strategy in Photovoltaic Boost Converter," Electric Power Components and Systems, Vol. 48, No. 2, 2021.

[5] H.C. Lu, and T.L. Shih, "Design of DC/DC Boost Converter with FNN Solar Cell Maximum Power Point Tracking Controller," IEEE Conference on Industrial Electronics and Applications, 2010.

[6] S. Gautam, D.B. Raut, P. Neupane, D.P. Ghale, and R. Dhakale "Maximum Power Point Tracker with solar prioritizer in Photovoltaic application," 5th International Conference on Renewable Energy Research and Applications (ICRERA), Birmingham, UK, 20-23 Nov, pp. 1051-1054, 2016.

[7] N. Genc, and I. Iskender, "An improved zero-voltage transition interleaved boost converter with high power factor," International Conference on Electrical and Electronics Engineering-ELECO, IEEE, 2009.

[8] R.K. Kharb, M.F. Ansari, and S.L. Shimi, "Design and Implementation of ANFIS based MPPT Scheme with Open Loop Boost Converter for Solar PV Module," International Journal of Advanced Research in Electrical, Electronics and Instrumentation Engineering, Vol. 3, No. 1, pp. 6517-6524, 2014.

[9] M.A. Zdiri, B. Bouzidi, O. Kahouli, and H.H. Abdallah, "Fault detection method for boost converters in solar PV systems," 19th International Conference on Sciences and Techniques of Automatic Control and Computer Engineering (STA), pp. 237-242, IEEE, 2019.

[10] A.I. Nusaif, and A.L. Mahmood, "MPPT Algorithms (PSO, FA, and MFA) for PV System Under Partial Shading Condition, Case Study: BTS in Algazalia, Baghdad," INTERNATIONAL JOURNAL of SMART GRID, Vol. 10, No. 3, pp. 100-110, 2020.

[11] A. BELKAID, I. COLAK, K. KAYISLI, and R. BAYINDIR, "Improving PV System Performance using High Efficiency Fuzzy Logic Control," 8th IEEE International Conference on Smart Grid, France, pp. 152-156, 2020.

[12] A. Sular, A. Mamzadeh, N. Genc, and M. Karaca, "PV Power Based Duty Cycle Control of Quasi-Resonant Inverter for Induction Cooking," 8th International Conference on Renewable Energy Research and Applications (ICRERA), Romania, 3-6 November, 2019.

[13] A. Belkaid, I. Colak, and O. Isik. "Photovoltaic maximum power point tracking under fast varying of solar radiation," Applied energy, Vol. 179, pp. 523-530, 2016.

[14] P. Sivakumar, A. Abdul Kader, Y. Kaliavaradhan, and M. Arutchelvi, "Analysis and enhancement of PV efficiency with incremental conductance MPPT technique under non-linear loading conditions," Renewable Energy, Vol. 81, pp. 543-550, 2015.

[15] E. Irmak, and N. Gler, "Application of a high efficient voltage regulation system with MPPT algorithm," International Journal of Electrical Power & Energy Systems, Vol. 44, No. 1, pp. 703-712, 2013.

[16] M. Karaca, N. Genc, A. Mamzadeh, and A. Sular, "Analysis of Passive Filters for PV Inverters Under Variable Irradiances," 8th International Conference on Renewable Energy Research and Applications (ICRERA), Romania, 3-6 November, 2019.

[17] L. Bouselham, M. Hajji, B. Hajji, A. El Mehdi, and H. Hajji, "Hardware implementation of fuzzy logic MPPT controller on a FPGA platform," In 2015 3rd International Renewable and Sustainable Energy Conference (IRSEC) (pp. 1-6). IEEE, 2015.

[18] T. Radjai, JP. Gaubert, L. Rahmani, and S. Mekhilef, "Experimental verification of P&O MPPT algorithm with direct control based on Fuzzy logic control using CUK converter," Int. J. Electr. Power Energy Syst., Vol. 25, No. 12, pp. 3492-3508, 2015.

[19] B. Buyukguzel, and M. Aksoy, "A current-based simple analog MPPT circuit for PV systems," Turkish Journal of Electrical Engineering & Computer Sciences, Vol. 24, pp. 3621-3637, 2016.

[20] A. Dolara, R. Faranda, and S. Leva, "Energy Comparison of Seven MPPT Techniques for PV Systems," Journal of Electromagnetic Analysis and Applications, Vol. 1, No. 3, pp. 152-162, 2009.

[21] N. Genc, H. Uzmus, and I. Iskender, "Dynamic Behavior of DC-DC Boost Converter Controlled with Cascade PIASC," 8th International Conference on Electronics, Computers and Artificial Intelligence (ECAI), 2016.

[22] A. Padmaja, and M. Srikanth, "Design of MPPT Controller using ANFIS and HOMER based sensitivity analysis for MXS 60 PV module," International Journal of Innovative Research in Advanced Engineering (IJIRAE), Vol. 11, No. 2, pp. 40-50, 2014

[23] M.F. Ansari, B.C. Sharma, and P. Saini. "Maximum Power Point Tracking of A Solar PV Module using ANFIS," The 3rd IEEE International Conference on Sustainable Energy Technologies, Nepal, 2012.

[24] A.A. Koochaksaraei, and Izadfar, H, "High-Efficiency MPPT Controller Using ANFIS-reference Model For Solar Systems," In 2019 5th Conference on Knowledge Based Engineering and Innovation (KBEI) (pp. 770-775). IEEE, 2019.

[25] A.M. Noman, K.E. Addoweesh, and A. I. Alolah, "Simulation and practical implementation of ANFIS-based MPPT method for PV applications using isolated Ćuk converter," International journal of Photoenergy, 2017.

[26] K. Boudaraia, H. Mahmoudi, and A. Abbou, "MPPT Design Using Artificial Neural Network and Backstepping Sliding Mode Approach for Photovoltaic System under Various Weather Conditions," International Journal of Intelligent Engineering and Systems, Vol. 12, No. 6, pp. 177-186, 2019.

[27] D. Sera, T. Kerekes, and R. "Teodorescu, Teaching maximum power point trackers using a photovoltaic array model with graphical user interface," In Proceedings on International Workshop on Teaching Photovoltaics, 2006.

[28] F. Masmoudi, F. Ben Salem, and N. Derbel, "Simple Models Design for One Mono-Crystalline Photovoltaic Cell by Identification of Internal Parameters," IEEE Annual Seminar on Automation, Industrial Electronics and Instrumentation (SAAEI 2014), Tangier/Marroc, 25-27 June 2014.

[29] H. Attia, "High performance PV system based on artificial neural network MPPT with PI controller for direct current water pump applications," International Journal of Power Electronics and Drive Systems, Vol. 10, No. 3, pp. 1329, 2019.

[30] F. Ben Salem, I. Bahri, H. Maamri, and al., "A Second-Order Sliding Mode Control of Switched Reluctance Motor," Electric Power Components and Systems, Vol. 48, No 6-7, pp. 640-651, 2020.

[31] V. Utkin, "Sliding Mode Control Design Principles and Application to Electric Drives," IEEE Trans. Industry Applications, Vol. 40, No. 1, pp. 23-36, 1993.

[32] K.D. Young, V.I. Utkin, and U. Ozguner, "A control engineers guide to sliding mode control," IEEE Trans. Control Systems Technology, Vol. 7, No. 3, pp. 328-342, 1999.